Defense Technical Information Center Compilation Part Notice

ADP011150

TITLE: Numerical Simulation of Adaptive Control Applicaton to Unstable Solid Rocket Motors

DISTRIBUTION: Approved for public release, distribution unlimited

This paper is part of the following report:

TITLE: Active Control Technology for Enhanced Performance Operational Capabilities of Military Aircraft, Land Vehicles and Sea Vehicles [Technologies des systemes a commandes actives pour l'amelioration des performances operationnelles des aeronefs militaires, des vehicules terrestres et des vehicules maritimes]

To order the complete compilation report, use: ADA395700

The following component part numbers comprise the compilation report:
ADP011101 thru ADP011178

Numerical Simulation of Adaptive Control Application to Unstable Solid Rocket Motors

M. Mettenleiter†, F. Vuillot‡ and S. Candel†

† *Laboratoire E.M2.C, CNRS, Ecole Centrale Paris, F-92295 Châtenay-Malabry Cedex*

‡ *ONERA Châtillon F-92322 Châtillon Cedex*

Abstract

This article describes current developments in the numerical simulation of active control. The objective of this investigation is to devise software tools for the development of active control. The present approach uses a numerical simulation of the system based on the Navier-Stokes equations. It differs from the more standard simulations relying on lower order dynamical models.

The main difficulties associated with the present strategy are related to the representation of the actuator in the flow simulation module and with the interfacing of this module with the adaptive control routine. These issues require careful treatment to obtain a suitable numerical model of flow control. It is first shown that the actuator may be described by a distribution of sources in the field.

The time stepping needed by the flow simulation module and by the control unit differ widely (the ratio between the time steps is of the order of 100 or more). This constitutes a source of perturbation and it may introduce unwanted high frequency components in the flow simulation. It is shown that this problem is alleviated by placing numerical filters at the controller input and output.

A set of calculations are carried out to simulate vortex shedding instabilities of a simplified solid propellant rocket. These instabilities are then adaptively controlled. This example serves to illustrate the simulation methodology and provides insights into the operation of the flow controller.

1 Introduction

Active control strategies have been mainly developed from experiments. More recent efforts have been directed at the computer simulation of control with the objective of testing and improving control algorithms. Numerical simulation complements experimentation and it has had considerable impact on the development of active flow control. The present investigation aims at devising reliable tools for the numerical simulation of active control. It adresses problems arising when one wishes to couple a flow simulation module and an adaptive control algorithm. The study is motivated by research directed at the control of vortex driven instabilities found in solid segmented rocket motors. Calculations are based on the solution of the Navier-Stokes equations using the Sierra software originating from ONERA. The flow simulation module has been used extensively to analyze vortex instabilities in configurations of interest in solid propellant propulsion. It is here used as a platform for active control. Numerical simulation is now more and more used to predict the behaviour of unstable subscale solid rocket motors. A recent example is given by Le Breton et al. [1], which already shows the interest of industry in this kind of simulation.

After a short review of the literature dealing with simulation of flow control (section 2), the flow simulation module is briefly described (section 3). One important aspect of the problem is to devise a suitable representation of an actuator or of a set of actuators. It is shown in the same section that this is best accomplished by distributing sources in the field. Modifications of the Sierra code are described and a series of open loop tests are carried out to show that the sources operate as expected. Problems related to the coupling of the flow simulation module with the control algorithm are considered in section 4. Specific issues arise because flow simulation and control require very different time sampling rates. The time step of the flow solver is much smaller than the sampling period of the controller. It is then necessary to take some precautions when dealing with the input and output of the control routine. The last section provides numerical simulations of vortex instabilities in a small rocket motor and control of these instabilities using an adaptive algorithm. Two situations

Paper presented at the RTO AVT Symposium on "Active Control Technology for Enhanced Performance Operational Capabilities of Military Aircraft, Land Vehicles and Sea Vehicles", held in Braunschweig, Germany, 8-11 May 2000, and published in RTO MP-051.

are considered. In the first the controller input is a pressure signal provided by a sensor located near the nozzle while the actuator is located near the motor head. In the second, the sensor is assumed to be sensitive to vorticity and the actuator is located near the point where the vortices are being shed. These two examples serve to show that the active control simulator is flexible and may be used to study the control strategy and examine the modification of the flow under control.

2 Previous studies dealing with simulation of active control

The simulation of active control of instabilities and noise may be divided in two main groups. One finds in the first group studies based on simplified dynamical models coupled to simple or more complex control schemes. A typical example from the field of sound and vibration control is due to Koshigoe. This author considers adaptive algorithms to reduce the noise from a confined cavity. Vibrations originating from outside the cavity walls may induce large pressure fluctuations in the cavity. The problem arises during space launchers take-off, the noise induced under the fairings may harm the payload and have detrimental effects on the future operation of the spacecraft. Koshigoe et al. [2] formulate a dynamical model of the system which is then used to test the filtered X-LMS algorithm with off-line identification of the secondary path [3]. On line identification is explored with the same model in a more recent study [4] and the LMS algorithm is compared to other control schemes [5] with regard to the convergence rate.

In the field of combustion instability Annaswamy et al. [6] develop a dynamical first order model of thermoacoustic interactions in a small laminar burner. This model is then used to design a controller and simulate its operation. The control algorithm is then used in the experiment. To account for changes in the system dynamics an adaptive controller is devised and compared with simulations carried out with an LMS algorithm [7].

Culick et al. [8] take into account linear and nonlinear coupling in their comprehensive dynamical model of instability. It is thus possible to describe some of the effects which lead to limit cycle oscillations found in practical systems. Fung et Yang [9] use this general formalism to design a PI controller of pressure oscillations in a combustion chamber. Annaswamy et al.[10] study the influence of mode coupling on controller design using the same general formulation. Koshigoe et al. [11] propose an adaptive algorithm with on-line identification to control a dynamical model of combustion instability.

In the second group of studies dealing with active control simulation, the flow is calculated by solving the Navier-Stokes equations. This provides a more realistic description of the flow dynamics and of the complex couplings taking place in practical devices. This approach uses the recent advances made in computational fluid dynamics. Menon [12] is perhaps the first to investigate active control in a large eddy simulation (LES) of a dump combustor typifying the geometry of a 2D ramjet. His controller uses a simple gain and phase applied to a pressure sensor signal and reinjected through a loudspeaker located at the backward facing step. Neumeier and Zinn [13] devise a special observer which identifies the unstable modes of a system. The modes are then amplified and phase delayed by a controller and reinjected into the computational domain. The balance equations are solved in one dimension.

Kestens [14] considers the adaptive (LMS) multiple channel control of aeroacoustic instabilities of cavities driven by an adjacent flow. The Navier-Stokes equations are solved in two dimensions. An actuator of the loudspeaker type or a pulsed jet is used to reduce the pressure level observed by different sensors.

Analysis of work belonging to this second group shows that some success has been reached but that the methodology needs further consolidation. It is our aim to devise a complete simulation of active control by coupling a non-steady Navier-Stokes solver with an adaptive controller. To reach this goal it is necessary to :

- Define a numerical representation of the actuator
- Study the actuator effect in open loop simulation tests
- Examine problems of controller interfacing

These different aspects are considered in the following sections.

3 The flow simulation module Sierra and the C1-geometry

The Sierra code is used to simulate the large scales of flow in order to analyze aeroacoustic instabilities generated in internal geometries found in solid rocket motors. The code operates in the planar or axisymmetric modes. It was designed by Vuillot [15] (see this reference for details on this platform). The Navier-Stokes equations are solved with a second order finite volume centered scheme. Time marching is explicit and uses the MacCormack predictor/corrector

method. Artificial viscosity is calculated with the Jameson method (see [16]). Simulations carried out in the present study do not use a subgrid model but the laminar viscosity has been augmented by a factor of 4 to dissipate the smaller scales of turbulence.

The code is used in what follows to simulate the flow in a specific geometry designated as C1. Parameters adopted in the simulations are gathered in table 1. Indices i et j specify locations of actuators and sensors with respect to the mesh. Figure 1 shows some positions in terms of their i-index.

The actuators will be defined as distribution of sources on the computational mesh. Their location is specified by the first and last values (i_d et i_f) of index i corresponding to the source and by the transverse size of the source specified in terms of elementary cells by index h. In the first case considered, the actuator sources are located on the first and second columns of cells composing the mesh and they occupy $h = 30$ cells in the transverse direction.

The computational domain is represented in Figure 1. The lower boundary 1 delivers a uniform stream of gases and represents the solid propellant surface. The mass flow rate per unit surface is imposed at this boundary, the gas temperature is prescribed and the tangential velocity component is zero at this limit. The boundary 2 represents the motor front head, the velocity vanishes on this boundary and the temperature is imposed. The line 3 is a symmetry plane. The outflow in section 4 is supersonic and numerical boundary conditions in this section are treated by simple extrapolation from the computational domain. At the wall 5 the flow velocity vanishes and the temperature is imposed.

This computational case was defined by ONERA to study the strong aeroacoustic oscillations resulting from vortex shedding from the propellant edge coupled with one of the modes of the system (see Lupoglazoff et Vuillot [17]). This constitutes a generic case, it is well documented and requires a limited amount of grid nodes (less than 10000) allowing long computational sequences.

In a first attempt at controlling the instabilities observed in the C1 case the actuator was simulated by a modified front end boundary condition. Perturbations were imposed on the incoming characteristic lines while outgoing waves were allowed to propagate out of the domain without reflection. Systematic tests carried-out in this situation indicated that the flow simulation did not respond adequately to the imposed fluctuations. For a given modulation frequency differing from that of the instability and for a small level of perturbation, one expects to find a superposition of acoustic waves in the system and a beating between these two waves if the frequencies are close. If that were the case it would have been possible to act on the signal delivered by the pressure sensor to control the vortex shedding. Calculations however indicated that beating was only produced at the beginning of the simulation and that vortices were very rapidly synchronized by the excitation signal introduced by the actuator. Closed loop control could not be achieved under these circumstances. This behavior was due to the modified boundary condition used to represent the actuator. Because the boundary did not reflect the incident waves the resonant properties of the system were changed and the vortex shedding phenomenon was altered.

It was then decided to use an alternative method to model the actuator. The boundary conditions were left untouched but source terms were distributed in the field. A somewhat similar approach was devised independently by Mohanraj et al. [18] who use sources in a one dimensional version of Euler's equations.

Without describing the details of the Sierra code, we only summarize the steps required to incorporate source terms in the balance equations.

- In the first step one has to define the number, location and type of source. This is done in a "driver" module which is read at the simulation beginning. This driver also contains information on the sensors used in the control scheme.
- During the calculation and at each time step the sources and sensors are updated.
- After each step the sources are added to the right hand side of the discretized balance equations.

If $\dot{\omega}_s$ designates the source of rate of mass addition per unit volume, the sources appear in the balance of mass, momentum and energy as follows :

$$\begin{aligned}
\rho^{n+1} &= \rho^{n+1} + \delta t \dot{\omega}_s \\
(\rho u)^{n+1} &= (\rho u)^{n+1} + (\delta t \dot{\omega}_s) u_s \\
(\rho v)^{n+1} &= (\rho v)^{n+1} + (\delta t \dot{\omega}_s) v_s \\
(\rho E)^{n+1} &= (\rho E)^{n+1} + (\delta t \dot{\omega}_s)(e_s + k_s)
\end{aligned}$$

Velocity components u_s, v_s and the internal energy of the injected stream e_s may be freely specified. The kinetic energy k_s is a function of u_s and v_s. In the present calculations a normalized value is adopted for the internal energy $e_s = 1$, and the velocities and kinetic energy u_s, v_s and k_s are set equal to zero.

The rate of mass addition $\dot{\omega}_s$ may be defined in various ways. In open loop tests this term takes the form

$$\dot{\omega}_s = a + b\sin(2\pi f t + \phi) + c\mathrm{sir}(f_1, f_2, dt).$$

This expression features a continuous component ($a \neq 0$), a sinusoidal modulation ($b \neq 0$) and/or a linear frequency modulation with a frequency sweep from f_1 to f_2 ($c \neq 0$). The source term $\dot{\omega}_s$ may also follow the active control output designated in what follows as "rac" :

$$\dot{\omega}_s = \text{rac}.$$

Tests of the source terms were carried out systematically to verify the proper operation of the concept. A constant section duct with closed/open left and right sections is filled with fluid. The mass flowing out of the tube exactly equals that injected by the sources.

In a second test a source was placed at various sections of the duct to excite the acoustic modes of the system. The mesh comprises in this case 61×20 nodes and the excitation frequency is that of the 3/4 wave mode.

The source was distributed over the height of the duct and occupied two cells in the axial direction. In the case shown in Figure 2 the source is located in the first and second cell which correspond to a pressure antinode. The acoustic mode develops uniformly in the transverse direction, the pressure and velocity distributions are exactly identical to those expected theoretically.

Other test cases show that the source terms incorporated in the Sierra code allow simulations of acoustic modulation without modification of the boundary conditions.

A second test series is now aimed at analyzing the response of the vortex driven flow in the C1 configuration under an external excitation. Parameters are those gathered in Table 1, case 1. The calculation begins with an established oscillation in the flow. Effects of different levels of source excitation are displayed in Figure 3.

The signal detected by the pressure sensor pfar2 is shown on the left. This signal will serve later as error signal in the control scheme for the first simulation. The signal detected by the differential pressure signal diff32 is shown on the right. Both signals feature the instability frequency. When the excitation amplitude is augmented two frequencies are detected, a further increase in amplitude leads to a decrease of the instability frequency level. Analysis of other sensor signals confirm this behaviour (for more detailed information, see [19]).

These calculations indicate that the C1 configuration responds to the new source terms placed in the field. The following points are noticeable :

- The instability phenomenon coexists with the frequency delivered by the actuator when the level of excitation is low.
- The frequency shifts towards the excitation frequency when the level of modulation is larger.
- The vortex shedding process is reorganized when the excitation frequency is very large.

Before describing closed loop calculations we now consider the control algorithm and examine issues related to interfacing.

4 Interfacing the control algorithm with the flow simulation module

The interface between the flow simulation module Sierra and the subroutine RAC which corresponds to the adaptive controller is designed to come as close as possible to a typical experimental configuration. The Sierra code is then used as a black box providing signals detected by different sensors and receiving the signal driving the actuator.

The integration step in the simulations is of $2.44\ 10^{-7}$ s, which corresponds to a sampling frequency $f_{\text{sierra}} = 4.096\ 10^6$ Hz. Results are recorded periodically every $d_w = 25$ Sierra time steps. The writing frequency is $f_{\text{write}} = 1.64\ 10^5$ Hz. It is not necessary and not recommendable to use the adaptive filter at these very high rates. Such frequencies would require extremely long filters in order to represent the system with sufficient precision. The filter renewal should be effected at a much lower rate, typically at a frequency $f_{\text{rac}} = 20480$ Hz. This value corresponds to the Sierra frequency divided by a factor $d_s = 200$.

To link a typical flow experiment featuring an analog sensor to the discrete control algorithm one uses an anti-aliasing filter. The same precaution seems necessary in connecting the flow simulation module Sierra to the control routine RAC. The sampling rate reduction by a large factor $d_s = 200$ induces a loss of information and may lead to problems of spectral overlap as those found when analog signals are sampled into discrete sequences. This justifies filtering of the controller input as shown in Figure 4.

The flow simulation module Sierra yields an input to the controller RAC at each integration step. One may then choose to keep each d_s value provided by Sierra or one may first low pass filter the values generated by Sierra and then keep the result every d_s sample.

A similar situation prevails at the controller output. One possibility is to use a "sample and hold" which keeps a constant value of the RAC output during the following d_s integration steps of SIERRA. Or

one may low pass filter the values in order to eliminate the high frequencies introduced by the successive jumps in the sampled and blocked values returned by the controller (see Figure 4).

The effects of filtering may be examined with the following tests. In a first trivial case (which is not shown here) $d_w = d_s = 25$. This means that the sensor values are written at the same frequency by SIERRA as they are updated and written by RAC. Hence, the sensor and actuator signals measured by RAC and SIERRA are identical.

In the second test case the sampling rates differ : $d_w = 25$ and $d_s = 200$. These values are later on adopted in the simulations with control. The corresponding results are now displayed on the left plot of Figure 5 (upper figure: actuator signal generated by RAC; second figure: pressure sensor measured by RAC; third figure: actuator signal measured by SIERRA; bottom figure: pressure sensor measured by SIERRA). The actuator signal measured by SIERRA clearly shows the discretisation effect. Sierra receives a discretized sinusoid (third curve from the top). The signal detected by the pressure sensor features high frequency oscillations which were not observed in the previous test. The high frequencies introduced by the sampled signal feeding the actuator interfere with the calculation. The controller input is formed by the samples without filtering (second plot from the top). High frequency components appear which perturb the signal and the initial frequency is less visible.

Using the same downsampling as in the previous test ($d_w = 25$ and $d_s = 200$) but including a low pass filter at the controller input and output one obtains the results shown on the right plot of Figure 5. The actuator signal seen by the Sierra sensor is smooth. The high frequency components in the pressure sensor signal are essentially suppressed. The controller input is noise free but a phase is introduced by the filter.

5 Active control simulation results

To control the C1 flow it is first necessary to identify the system seen by the controller. With this information the controller filter may be brought to convergence to a steady solution

5.1 Secondary path identification

Off-line identification is used in the context of this simulation to describe the secondary path. As in experiments it is possible to get this information in two regimes of operation :

- Identification may be carried out in the presence of the vortex instability phenomenon.
- Identification may be carried out in the absence of vortex shedding. This is achieved by multiplying the viscosity by a factor which is typically of the order of 20

During identification, the controller RAC delivers a frequency which varies linearly in time (a siren signal). The signal detected by the pressure sensor (pfar2) is recorded by RAC and Matlab is used to calculate an IIR filter comprising 21 coefficients in the numerator and denominator.

Figure 6 displays the results obtained in the two cases. On the left the secondary path is estimated in the presence of vortex shedding. On the right, the vortices are suppressed. In this second case the peak in amplitude corresponding to the instability amplitude is reduced to a great extent and this is also true for a second peak around 1800 Hz. The phase also changes notably as the viscosity coefficient is augmented. The filters reproduce the real behavior quite well.

On physical grounds it seems more appropriate to use the identification result obtained in the presence of the vortex shedding process. The corresponding secondary path transfer function is used in what follows.

5.2 Adaptive control

The NSC (Noise Source Control) algorithm described in [20] or [19] is used in the simulations presented in this section. The control loop is closed when the flow simulation has reached a limit cycle with a well established vortex shedding instability. Figure 7 shows the time evolution using different sensors after the controller is switched on. This event is represented by a vertical line. The error signal (pressure sensor pfar2) is shown on the top left. A considerable reduction is observed in the beginning but the algorithm does not converge to a steady state. A stationary solution is reached after a transient phase featuring short modulations. The actuator signal shown at the bottom left also features pulsations before converging to a steady state. One also notices that a large amplitude is initially generated to act on the process. This amplitude diminishes later and converges to a lower level when the signal becomes stationnary. This behaviour is also observed in experiments (see [20]) suggesting that the controller acts on the vortex shedding process which drives the oscillation in the system.

This interpretation is confirmed by the velocity signal u2far2 shown at the right and at the bottom of

Figure 7. After an initial phase with modulations the amplitude is stabilized at a lower level. The frequency also changes and the shift during the transition may be at the source of modulations detected by all the sensors.

Finally, the pressure sensor pfav placed on the motor front end (displayed on the right and at the top of Figure 7) features a notable reduction of amplitude when the controller is on but it is worth recalling that this signal is not used in the control process.

The power spectral densities calculated during steady state operation confirm the controller influence on the instability phenomenon. Figure 8 shows on the left the spectral density of the pressure signal pfar2 without and with control.The component at the instability frequency vanishes completely (> 40 dB) but a new peak appears at a different frequency at a much reduced level (factor of 10).

The spectral density of the velocity signal u2far2 can be seen on the right of the same Figure. It clearly shows that the oscillation is shifted to a higher frequency. The initial peak has disappeared. The new component reaches a significantly reduced level (factor 3). This peak at 3900 Hz is close to the 3L mode of the C1 configuration and it may excite an acoustic oscillation at that frequency (this explains the small peak appearing in the left in Figure 8).

A similar behaviour can be observed for the pressure signal pfav. The peak at the initial frequency vanishes and the phenomenon is shifted to the higher mode. The overall level is reduced by a factor of 3. These results are not shown here.

The controller does not suppress the vortex shedding but it shifts the phenomenon to another eigenmode. The intensities at this new frequency are nevertheless significantly reduced.

The vorticity field before and after control is shown in Figure 9. The lower image corresponding to the controlled operation shows that coherent vortices are still present but their size and shedding frequency are modified in agreement with observations of the velocity spectral density.

It appears that in the numerical simulation the vortex shedding is more persistent than in the experimental case. This could be explained by the difference in the broad band content of the signals detected in the two situations. Without coupling the acoustic signal is submerged in the broad band noise existing in the experimental facility and it cannot trigger the vortices in a coherent fashion. The shedding takes place more randomly (this is demonstrated in experiments described in [19]) or it may even be completely suppressed as described by Huang and Weaver [21]. In the numerical simulation, the flow conditions are much "cleaner". There is no broad band noise which could prevent the synchronization between acoustics and vortex dynamics. The vortices find in all circumstances a phase reference even when the acoustic signal level is strongly reduced.

In the case examined the controller acts on the acoustics and then indirectly through coupling on the vortex shedding. A more efficient reduction of velocity fluctuations could be obtained by acting directly on the shear layer. It is interesting to see if an additional decrease in the signal amplitude could be obtained with a new arrangement in which the actuator is set at the edge of the propellant surface (case 2 in Table 1) and the sensor provides a vorticity signal.

After identification of the secondary path corresponding to this new set-up (with vortex shedding) a new simulation is carried out. Figure 10 shows the pressure signal pfar2 (top left) and pfav (top right). The actuator signal is at the bottom left of figure 10. The velocity sensor u2far2 appears at the bottom right. Reduction of this last signal is effectively more direct than in the previous calculation (compare Figures 7 and 10). The pressure sensors also behave in a different manner. The pressure levels are first slightly augmented, reduction taking place in a second stage (Figure 10). The same increase is observed in the velocity fluctuation for the first simulation (Figure 7).

The reduction in amplitude obtained in the steady state may be compared to that obtained previously. In general, the same frequency shift can be observed as in case 1. The initial peaks disappear and the phenomenon is shifted to the 3L mode, where it reappears with largely reduced levels. The spectral densities of the different signals are shown in Figure 11. The pressure signal pfar2 is slightly lower in case 1 than in case 2. This is not surprising since this signal is to be minimized in the first arrangement. In case 2, the pressure level at the front end is lower and the velocity fluctuations u2far2 are diminished by a factor of 4.5. The overall reduction in the error sensor (a vorticity signal) is also considerable. As for the other sensors, the initial frequency has disappeared and the 3L peak appears with a level reduced by a factor 6.3 (this result is not shown here). It is also worth noting that convergence in the second case is smoother perhaps because the controller acts more directly on the instability process.

It is interesting to note that between $t = 0.12$ et $t = 0.14$s all signals are reduced significantly (see Figure 10). This reduction is unfortunately not maintained and the signals reach a steady state at a greater level. There are some possible reasons for this behavior. The frequency shift drives the controller towards a new solution. As the sensor level is greatly reduced,

the rate of convergence for this new situation is diminished (a factor of 10 reduction in amplitude reduces the convergence rate by a factor of 100). One may also invoke the fact that the sensor signal is too "clean". In the numerical calculation the error signal e detected by the sensor cannot be driven to zero because this would not lead to a steady state of the controller (see [20] or [19] for more details). The controller action would tend to zero but with a vanishing output the instability mechanism will not be controllable. This scenario requires further testing.

Figure 12 shows the vorticity distribution at a point in time ($t = 0.1264s$) where the level of fluctuations is quite small. Coherent vortices have essentially disappeared from the flow-field and the shear layer develops without roll-up.

6 Conclusions

The simulation of active control is investigated in this article. A Navier-Stokes solver is coupled to an adaptive control algorithm. It is shown that the actuator may be defined by distributing sources in the computational domain. This method is first used in open loop tests. The coupling of the flow simulation module with the control algorithm is then considered. Because the rates of operation of the flow solver and active control are widely different the signals at the controller input and output must be filtered. It is shown that this eliminates high frequency components which would otherwise perturb the calculation. The simulation of active control is then developed in a solid rocket motor geometry in which vortex shedding takes place which leades to acoustic resonance of the system. Results obtained demonstrate that control is feasible and that the method may be used to examine the changes in the flow field induced by the controller.

Acknowledgment

This work was supported in part by the CNES. It is part of the ASSM research programme coordinated by CNES and ONERA.

References

[1] P. Le Breton, J.-F. Guéry, F. Vuillot, and M. Prévost. Recent advances in the prediction of SRM thrust oscillations. In *Premier Colloque Européen sur la Technologie des Lanceurs "Vibration des Lanceurs, Toulouse"*, 1999.

[2] S. Koshigoe, J. T. Gillis, and E. T. Falangas. A new approach for active control of sound transmission through an elastic plate backed by a rectangular cavity. *J. of the Acoustical Society of America*, 94(2):900–907, 1993.

[3] S. Koshigoe, A. Teagle, and A. Gordon. A time domain study of active control of sound transmission due to acoustic pulse excitation. *J. of the Acoustical Society of America*, 97(1):313–323, 1995.

[4] S. Koshigoe, A. Teagle, C.-H. Tsay, S. Morishita, and S. Une. Numerical simulation of active control with on–line system identification on sound transmission through an elastic plate. *J. of the Acoustical Society of America*, 99(5):2947–2954, 1996.

[5] S. Koshigoe, A. Teagle, and C.-H. Tsay. A rapidly convergent adaptive controller applied to suppresion of random noise transmission. *Journal of Vibration and Acoustics*, 120:449–454, 1998.

[6] A. M. Annaswamy, M. Fleifil, J. W. Rumsey, J. P. Hathout, and A. F. Ghoniem. An input-output model of thermoacoustic instability and active control design. Technical Report No. 9705, MIT, 1997.

[7] A. M. Annaswamy, O. M El Rifai, M. Fleifil, J. P. Hathout, and A. F. Ghoniem. A model–based self–tuning controller for thermoacoustic instability. *Combust. Sci. and Tech.*, 135:213–240, 1998.

[8] F. E. C. Culick, W. H. Lin, C. C. Jahnke, and J. D. Sterling. Modeling for active control of combustion and thermally driven oscillations. In *Proceedings of the American Control Conference, Boston MA*, 1991.

[9] V. Yang Y.-T. Fung. Active control of nonlinear pressure oscillations in combustion chambers. *J. Prop. and Power*, 8(6):1282–1289, 1992.

[10] A. M. Annaswamy, M. Fleifil, J. P. Hathout, and A. F. Ghoniem. Impact of linear coupling on the design of active controllers for the thermoacoustic instability. *Combust. Sci. and Tech.*, 128:131–180, 1997.

[11] S. Koshigoe, T. Komatsuzaki, and V. Yang. Active control of combustion instabilities with on–line system identification. In *34th. Aerospace Sciences Meeting & Exhibit, Reno, Jan. 15–18.* AIAA Paper 96-0759, 1996.

[12] S. Menon. Active combustion control in a ramjet using large-eddy simulations. *Combust. Sci. and Tech.*, 84:51–79, 1992.

[13] Y. Neumeier and B. Zinn. Active control of combustion instabilities using real time identification of unstable combustor modes. In *Proceedings of the IEEE Conference on Control Applications*, pages 691–698, 1995.

[14] T. Kestens. *Etude numérique du contrôle adaptatif multivoies des instabilités aéroacoustiques des cavités.* PhD thesis, Institut National Polytechnique de Toulouse, 1999.

[15] N. Lupoglazoff and F. Vuillot. Two-dimensional numerical simulation of the stability of a solid propellant rocket motor. In 29^{th} *Aerospace Science Meeting, Reno, USA*. AIAA Paper 91-0205, January 7–10 1991.

[16] A. Jameson and W. Schmidt. Some recent developments in numerical methods for transonic flows. *Computer Methods in Applied Mechanics and Engineering*, 51:467–493, 1985.

[17] N. Lupoglazoff and F. Vuillot. Numerical simulations of vortex shedding phenomenon in 2D test case solid rocket motors. In 30^{th} *Aerospace Sciences Meeting.* AIAA Paper 92-0776, 1992.

[18] R. Mohanraj, Y. Neumeier, and B. T. Zinn. Characteristic-based treatement of source terms in euler equations for roe scheme. *AIAA J.*, 37(4):417–424, 1999.

[19] M. Mettenleiter. *Contrôle adaptatif des instabilités aéroacoustiques. Application aux systèmes de propulsion.* PhD thesis, Ecole Centrale Paris, 2000.

[20] M. Mettenleiter, E. Haile, and S. Candel. Adaptive control of acroacoustic instabilities. *J. Sound Vib.* (in press), 2000.

[21] X. Y. Huang and D. S. Weaver. On the active control of shear layer oscillations across a cavity in the presence of pipeline acoustic resonance. *J. Fluids and Structures.*, 5:207–219, 1991.

Number of grid points	318×31
Pressure sensor pfar1 (i, j)	210,1
Pressure sensor (error measure, case 1) pfar2 (i, j)	245,1
Pressure difference sensor diff32	pfar2-pfar1
Forward plane pressure sensor pfav (i, j)	1,30
x-velocity sensor u2far2 (i, j)	245,24
Vorticity sensor (error measure, case 2; i, j)	245,24
Actuator position, case 1 i_d, i_f, h	1,2,30
Actuator position, case 2 i_d, i_f, h	64,74,5
Reference length	0.47m
Reference velocity	1075.37 m/s
Integration time step	1/4.069e+6 = 2.4414e-7 s
Excited acoustic mode frequency (close to 2L)	2540 Hz

Table 1: Parameters of the C1 computations .

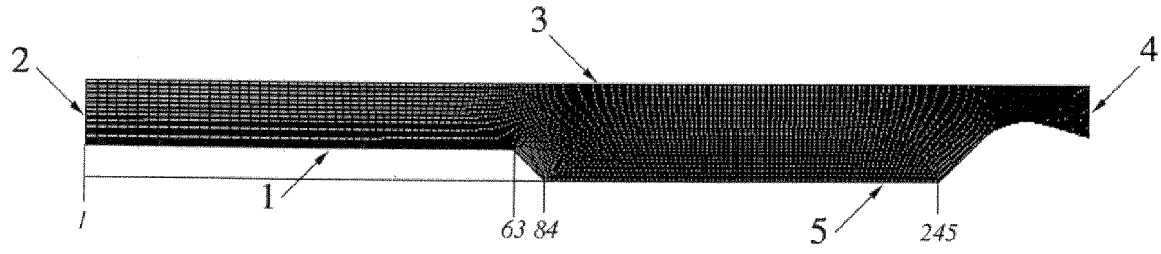

Figure 1: The C1 computational domain.

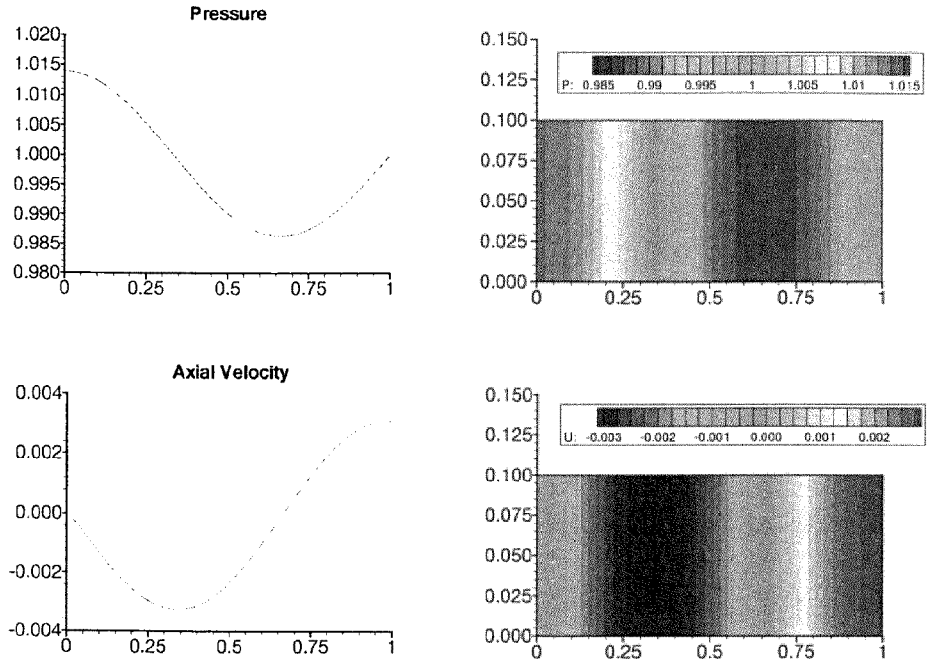

Figure 2: Excitation at a pressure antinode. At the top : pressure signal. At the bottom : acoustic velocity signal.

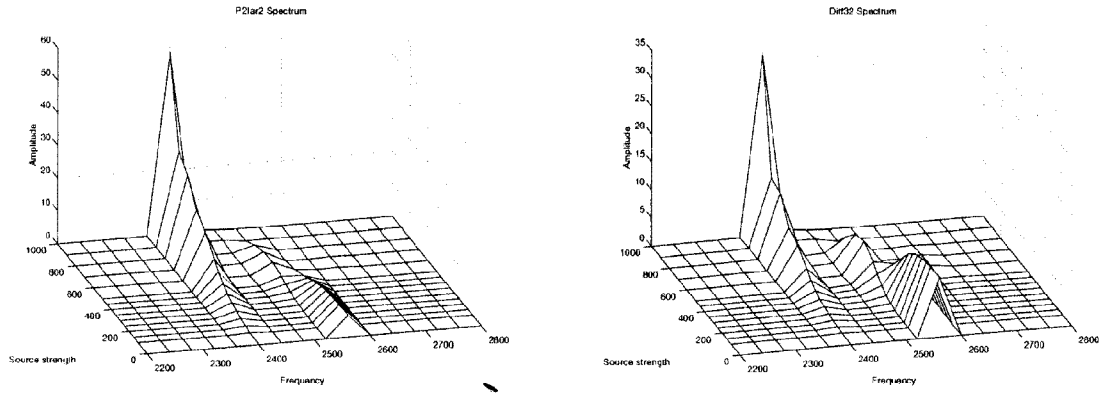

Figure 3: Influence of a single acoustic source on the pressure signal detected by the pfar2 error sensor (left) and by the differential sensor diff32 (right). The level of excitation varies from low to high.

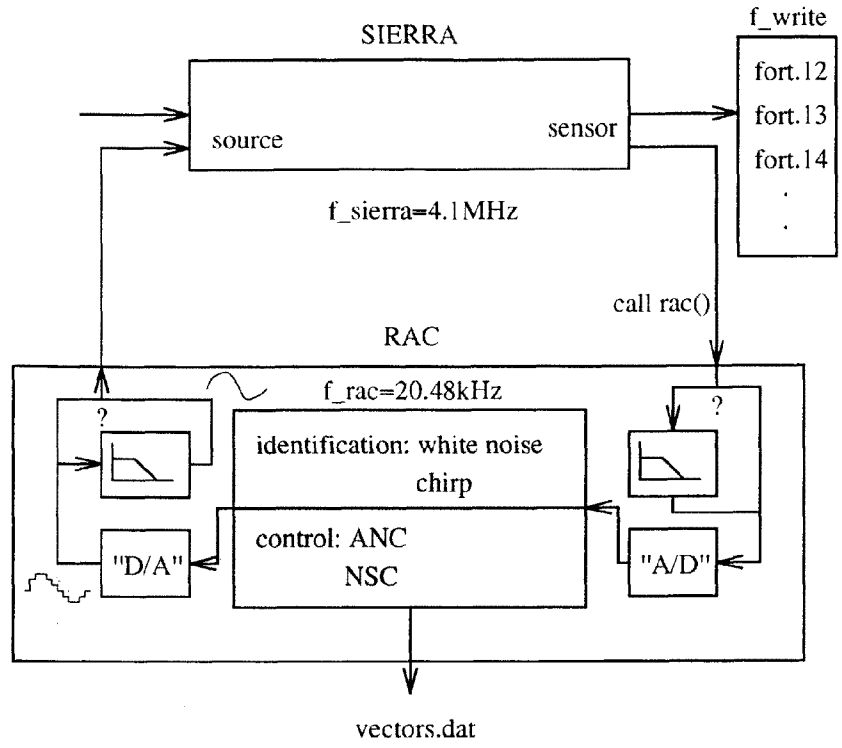

Figure 4: Diagram of the Sierra interface with the adaptive controller RAC

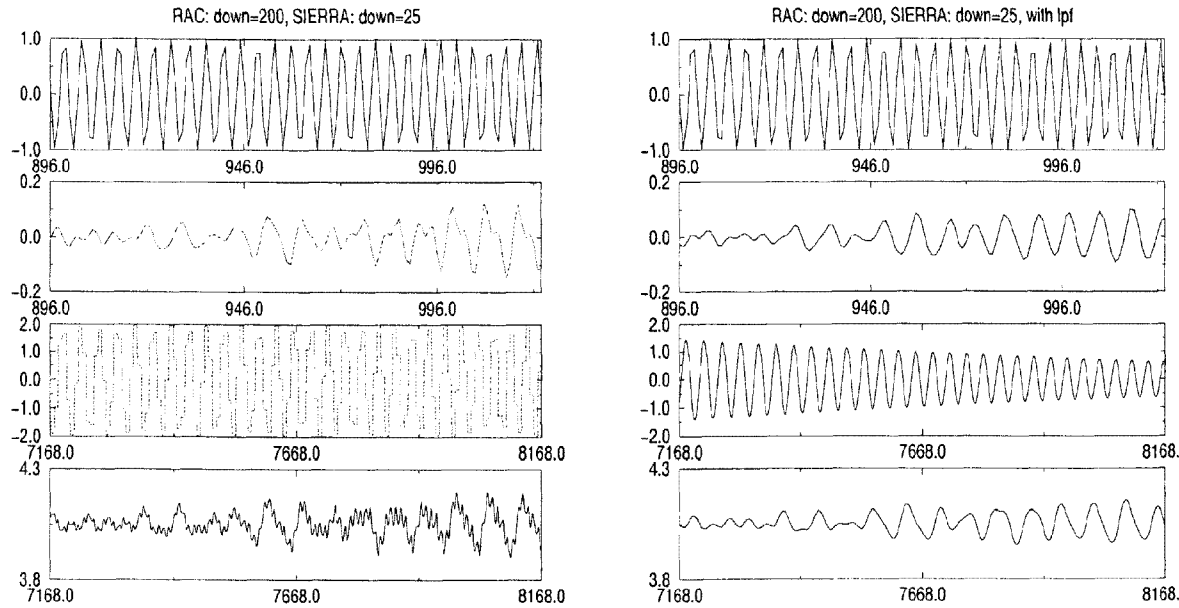

Figure 5: Comparison between actuator/sensor in RAC (top) and SIERRA sensors (bottom), $d_w = 25$, $d_s = 200$. Left: no filtering. Right: with filtering.

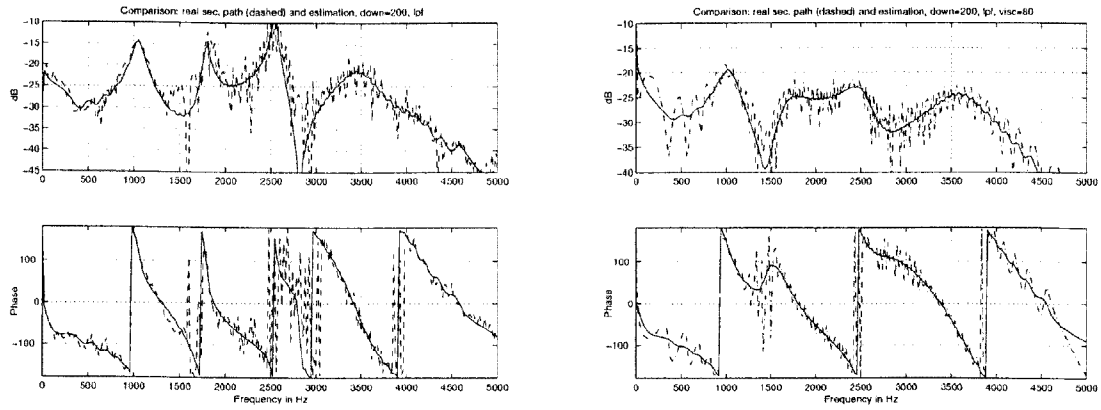

Figure 6: Real (—·—) and estimated (——) secondary path IIR filter (21/21). On the left, identification is carried out in presence of vortex shedding. On the right identification is carried out with an augmented viscosity coefficient.

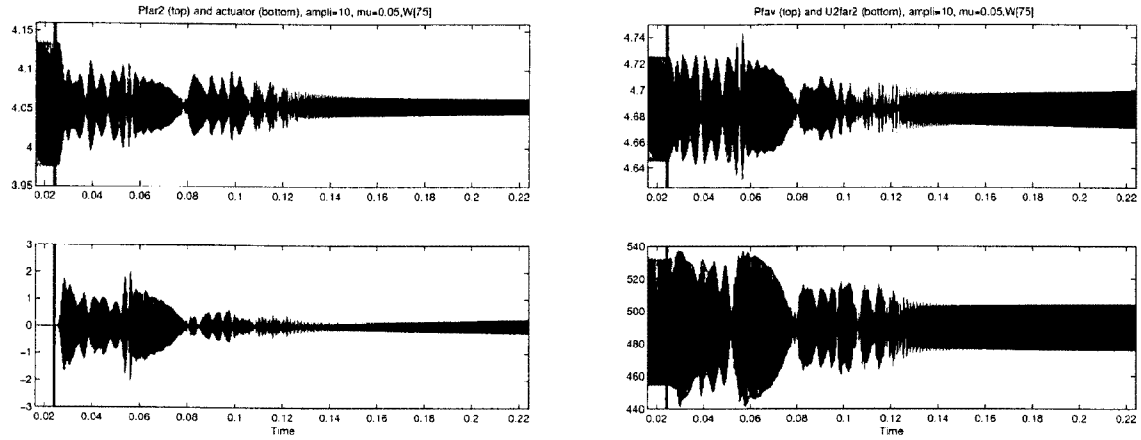

Figure 7: Control results. On the left and top : error sensor pfar2, left and bottom : actuator signal. On the right and top : pressure sensor pfav, on theright and bottom : velocity signal u2far2. The vertical line indicates that the controller is switched on.

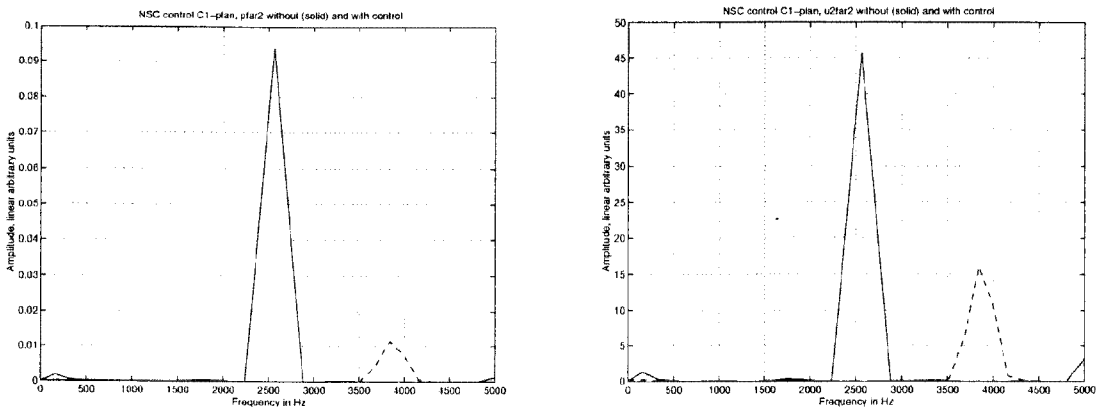

Figure 8: Control results. On the left:power spectral density of pfar2, on the right power spectral density of u2far2. Without control (——) and with control (----).

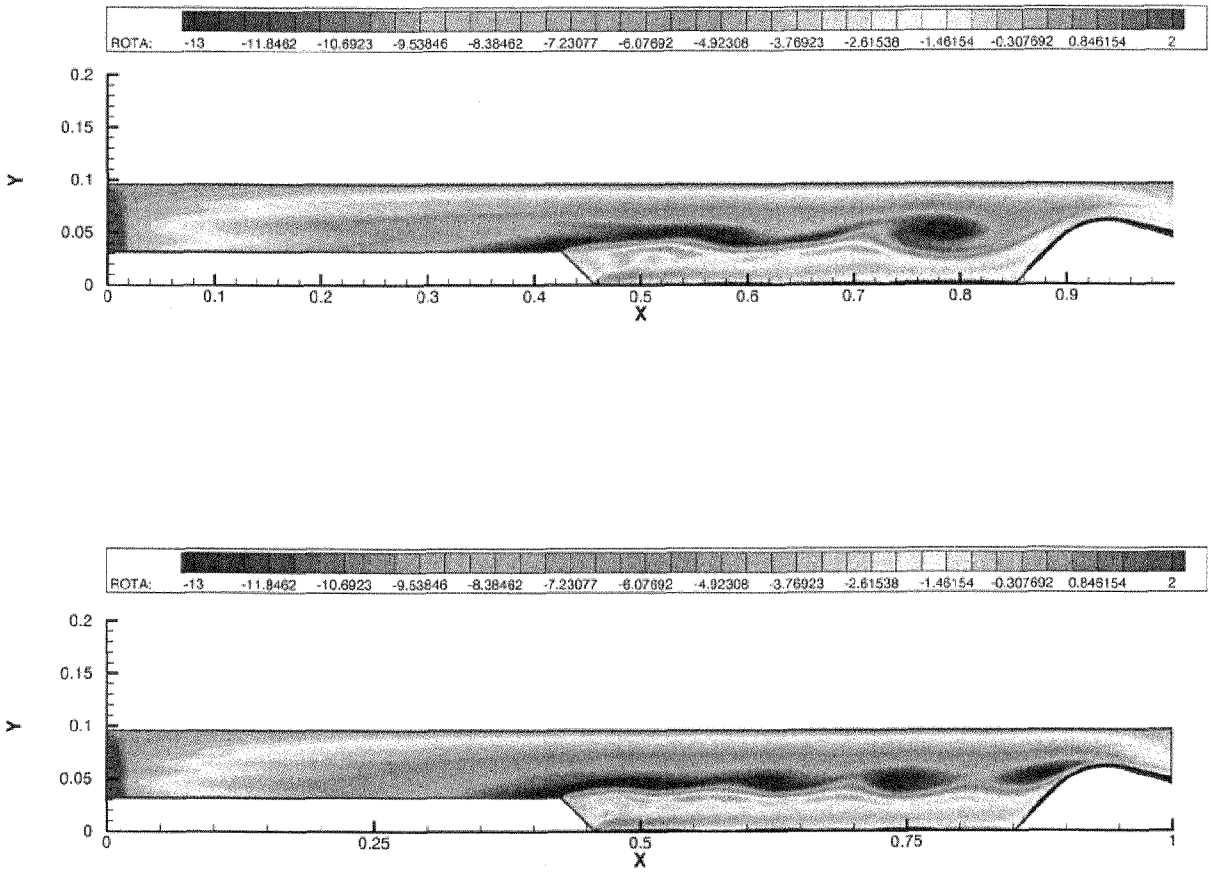

Figure 9: Vorticity field before (top) and after (bottom) control The controller input is the pressure signal pfar2 (case 1).

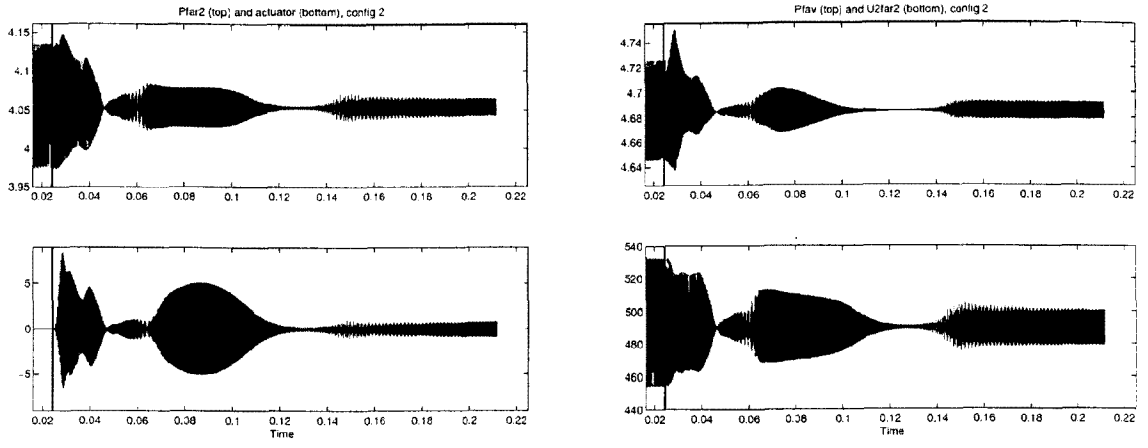

Figure 10: Control results obtained in case 2. A vorticity sensor provides the input to the controller. Top left : pressure sensor pfar2. Bottom left : actuator signal. Top right : pressure sensor pfav. Bottom right : velocity signal u2far2. The vertical line indicates control switch on.

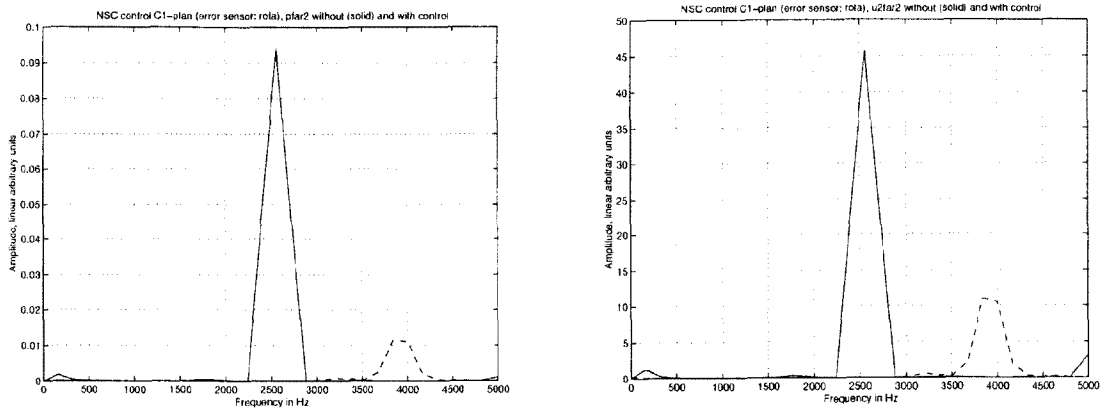

Figure 11: Control results obtained in case 2. A vorticity sensor provides the input to the controller. Left : pfar2 spectral density right : u2far2 spectral density. With (———) and without (- - - -) control.

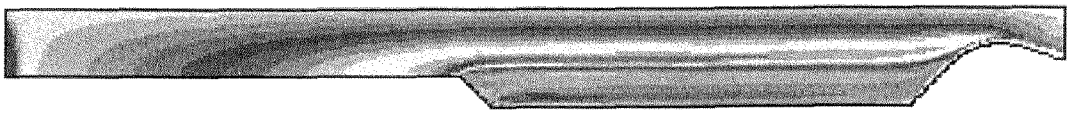

Figure 12: Vorticity field at $t = 0.1264s$. Control is achieved with a vorticity sensor and an actuator located at the propellant surface edge (case 2)

PAPER -7, M. Mettenleiter

Question (M. Huth, Germany)

Which kind of practical system can represent the modeled actuator and which parameters of the actuator driver were optimized by the adaptive controller?

Reply

The modeled actuator represents a mass injector in the numerical simulation. The corresponding velocities and the internal energy of the added mass were specified. In practical systems, this corresponds to a propellant injector.

The adaptive controller phase shifts and amplifies the sensor signal before it is re-injected by the actuator. The appropriate phase shift and amplification (which changes for different instability frequencies) is determined by the adaptive scheme.